International Journal of Mathematical, Engineering and Management Sciences
Vol. 5, No. 6, 1210-1233, 2020
https://doi.org/10.33889/IJMEMS.2020.5.6.091

Behavior of Curved Steel-Concrete Composite Beams Under Monotonic Load

Abdulkhaliq A. Jaafer
Department of Civil Engineering,
Misan University, College of Engineering, Maysan, Iraq.
Corresponding author: aljabery@uomisan.edu.iq

Saba L. Kareem
Department of Civil Engineering,
Misan University, College of Engineering, Maysan, Iraq.
E-mail: sa.alkaabi12555@gmail.com; saba94@uomisan.edu.iq

(Received February 12, 2020; Accepted June 9, 2020)

Abstract
The paper develops a numerical investigation on the behavior of steel-concrete composite beam curved in plan to examine the effect of the various parameters. Three-dimensional finite element analysis (FEA) is employed using a commercial software, ABAQUS. The geometric and material nonlinearities are utilized to simulate the composite beam under a monotonic load. The FEA efficiency has been proved by comparing the numerical results with experimental tests obtained from previous literature, including load-deflection curves, ultimate load, ultimate and failure deflection, and cracks propagation. The validated models are used to assess some of the key parameters such the beam span/radius ratio, web stiffeners, partial interaction, concrete compressive strength, and steel beam yield stress. From the obtained results, it is noticed that the span/radius of curvature ratio influences the loading capacity, the beam yielding (i.e. the beam yield at an early stage) when the span/radius ratio increases and inelastic behavior developed early of the beam due to the torsional effect. The presence of web stiffeners with different locations in the curve composite beam affected the shear strength. The web twisting and vertical separation at the beam mid-span are observed to decrease as the number of the stiffeners increase due to the decrease in the beam torsion incorporating with transferring the failure to the concrete slab. Furthermore, the partial interaction and steel beam yield stress developed in this study appear to have a remarkable effect on beam capacity.

Keywords- Composite beam, FEA modeling, Web stiffeners, Partial interaction, Span/radius ratio, Vertical separation.

1. Introduction

Recently, conventional composite steel-concrete construction is vastly utilized around the world as one of the most economical constructions in the civil engineering structures. It is commonly employed in contemporary high-way bridges and buildings for decades due to its useful characteristics of combining the two components of composite construction compared to the reinforced concrete construction. Members curved in plan have been dramatically employed in modern constructions such as highway bridges, interchanges and balconies in an urban area for aesthetics, economic and structural purposes. As a result of asymmetrical loading or complexity of member geometry, twisting moment combined with flexural moment has been developed in such members. However, due to the complexity of stress state, a prediction of strength and structural behavior of members curved in plan under the combined action of bending and twisting moments may be tricky to fulfill. The available international codes such as AISC (2006) and Eurocode 4 (2005) do not cover these combined effects. Challenges in the design and construction of curved composite members with increased demand have made it necessary to conduct a study to understand the behavior of these members. On other hand due to the high complexity of geometry

International Journal of Mathematical, Engineering and Management Sciences
Vol. 5, No. 6, 1210-1233, 2020
https://doi.org/10.33889/IJMEMS.2020.5.6.091

and material nonlinearities of the curved composite member, the familiar analytical method and an exact solution are very difficult if not impossible in some cases. Since experimental studies for such type of structures are expensive and time consuming, the researchers have been conducting numerical modeling or finite element tests in dealing with this issue.

Many researchers have adopted numerical studies to explore the behavior of curved steel and steel–concrete composite members. Yang and Kuo (1987) derived a differential equation based on the principle of virtual displacement with a continuum mechanics basis, to explore the curved beam buckling behavior under various loading actions and curvature effect. Liew et al. (1995) presented a numerical study carried out using ABAQUS for analyzing I-steel beams, which are curved in horizontal plane under inelastic large-displacement behavior. The results of the finite element model are employed to propose an approximate equation and standard charts for determining the strength capacity of such beams. Pi and Bradford (2000) developeds an extensive 3D finite element analysis by ABAQUS software for I-steel beam curved in plane under equal bending moment with the inclusion of curvature effect. The numerical simulations emphasized that when the initial curvature increases both non-uniform torsion and bending begin to dominant intensively, and the nonlinear inelastic behavior develops early. A numerical analysis was developed by Thevendran et al. (1999) using ABAQUS to predict the loading capacity and nonlinear behavior of a curved composite member. The concrete slab and steel girder simulated a using shell element, and the stud shear connector was simulated using a rigid beam element. The validation process was carried out on five test specimens using the earliest experimental study that has been tested by Thevendran et al. (2000). The finite element results showed a close agreement comparing with the experimental test results. In addtion, Kim et al. (2007) discussed the full nonlinear behavior of transverse stiffeners in straight and I-girder curved in horizontal plan bridges by finite element analysis. A proposed design equation was recommended for transverse stiffeners' strength and flexural stiffness. From the outcome results, a more important consideration was demonstrated in developing shear post-buckling resistance than the satisfaction of an area or axial force requirement. Otherwise, it was found that regardless of the type of the stiffeners, girders with a given slenderness and web panel aspect ratio had essentially the similar strength if they are designed based on the suggested equations. Erkmen and Bradford (2009) extended numerical analysis using ABAQUS program with the elastic total Lagrangian formulation for deriving the composite beam strain expression. The nonlinearity of geometry and partial interaction at the interfaces are considered. The results demonstrated that the formulation was effective and accurate to captivate the behavior of such beams with high effectiveness finite element (FE). The proposed formulation has been extended and compared with experimental results to investigate time-dependent shrinkage and creep of curve composite members by Erkmen and Bradford (2011a, b) and Liu et al. (2013a, b).

A study considered the effect of material's and geometry nonlinearities of a composite beam has been carried out numerically by Liu et al. (2013c). The efficiency of the numerical model was compared with experimental results, taken into account the effect of partial interaction and initial curvature on the curved composite beam non-linear inelastic analysis. Tan and Uy (2009) reported an experimental test to explore the ultimate strength of the curved composite beam under a single load applied at mid-span with different span/radius of curvature ratio. Bending-torsion moments interaction curves are presented for a curved in plan composite beam with partial and full interaction. Moreover, another study of the curved composite beams was numerically investigated by Tan and Uy (2011). ABAQUS software was utilized to predict the combination of flexural and twisting moments of these members. A new phenomenon called torsion induced vertical slip has

International Journal of Mathematical, Engineering and Management Sciences
Vol. 5, No. 6, 1210-1233, 2020
https://doi.org/10.33889/IJMEMS.2020.5.6.091

been developed, at which the assumption of plane section remains plane was invalidated. Lin and Yoda (2014) developed a numerical analysis on steel-concrete curved composite beams under hogging moment effect. The load carrying capacity and strength, distribution of sectional strain, moving the neutral axis before and after cracking of composite beam, and the longitudinal reinforcing bars strain are investigated. Furthermore, the interaction equation between the torsional moments and the ultimate bending was also proposed. Issa El-Khoury et al. (2014) developed numerical analysis by ABAQUS program to determine longitudinal stiffeners optimal locations by a series of parametric studies to increase the flexural strength of doubly symmetric plate girders which are curved in horizontal plan. It was found that the optimal position for longitudinal stiffeners on a curved web in horizontal appreciably does not appear from that recommended AASHTO LRFD for a straight web. Otherwise, it was found for slender webs (D/t_w= 300) at higher girder radii the most significant way to enhancing the flexural capacities of the curved girder was by providing longitudinal stiffeners. Zhang et al. (2015) presented 3-D finite element models using MIDAS program seeking torsional on curved composite beams behavior in the construction stage.

Since the available studies that dealing with the behavior of curved in plan steel-concrete composite beam are insufficient, many further studies are still needed to understand the influences of some parameters on the behavior and carrying capacity of composite beams. The main goal of this study is to develop a three-dimensional finite element analysis of curved steel-concrete composite beam using ABAQUS. To fulfill the objectives of the study, firstly the ultimate strength and load-deflection relationships, as well as the crack patterns, are validated with the corresponding experimental results from the previous study carried out by Tan and Uy (2009). Moreover, a parametric study that is not well covered in literature is accomplished to investigate the effects on the composite steel-concrete beams performance of transverse web stiffeners, concrete slab compressive strength, yield stress of steel beam, shear connectors and radius of curvature.

2. Description of the Tested Model

The experimental results of the composite steel—concrete beam curved in a plan conducted by Tan and Uy (2009) are investigated in the present study. Three curved composite beams designed as simply supported, identified as CCBP-1, CCBP-2 and CCBP-3, and are designed by them with partial shear connection. The load was applied at the beam mid-span. The beams are 6200 mm in length and simply supported at 6000 mm. The specimens are constructed of a concrete slab with a 500 mm width (b_c) and 120 mm depth (t) connected to a rolled steel beam (Type 200UB29.8) with a section of 207 mm (beam depth h_s) × 134 mm (flange width b_f) × 9.6 mm (flange thickness t_f) × 6.3 mm (web thickness t_w). Headed shear studs are welded in a single row to the top surface of the steel flange with a diameter, length, and spacing of 19, 100, and 450 mm, respectively. Reinforcements of diameters 10 mm and 12 mm are placed on the concrete slab for torsional and longitudinal reinforcement, respectively. The yield stress of 10 mm and 12 mm steel reinforcement, the steel beam web and flange are, 500, and 347 MPa, respectively. The nominal compressive strength of the concrete slab was 38 MPa. Further details of the specimens are demonstrated in Figure 1 and Table 1.

International Journal of Mathematical, Engineering and Management Sciences
Vol. 5, No. 6, 1210-1233, 2020
https://doi.org/10.33889/IJMEMS.2020.5.6.091

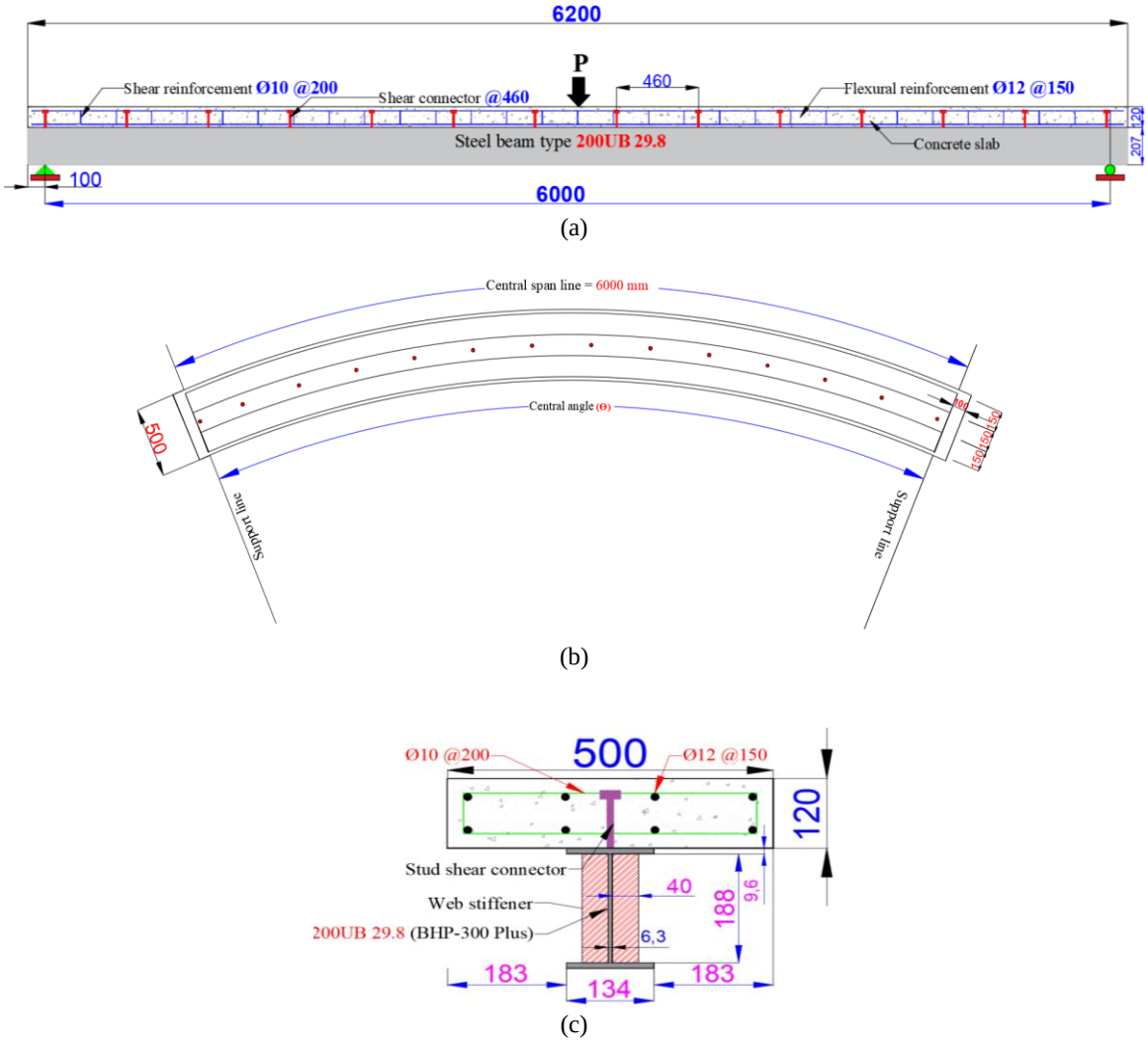

Figure 1. Geometry and dimensions of the curved composite steel—concrete beams CCBP-1, CCBP-2 and CCBP-3 (unit: mm): (a) Side view, (b) Plan, (c) Cross-section

Table 1. Details of the specimens of steel-concrete composite beam curved in plan.

Specimen no.	Central angle (°)	Span/Radius	Radius (m)	Degree of shear connection (%)	Stud spacing (mm)	Lever arm (mm)
CCBP-1	15.77	0.275	21.8	50	460	220
CCBP-2	16.85	0.294	20.4	50	460	235
CCBP-3	26.04	0.455	13.2	50	460	362

3. Finite Element Model

Although laboratory tests provide valuable results, they cannot be carried out to cover a wide range of variables because it is entailing expensive equipment and instruments in addition to a specialized laboratory with skilled technicians for completing the experiments. Therefore, to expand the range

International Journal of Mathematical, Engineering and Management Sciences
Vol. 5, No. 6, 1210-1233, 2020
https://doi.org/10.33889/IJMEMS.2020.5.6.091

of the parameters to be studied, the most appropriate tool for this purpose is the finite element method FEM. In this study, 3-D finite element models using commercial software ABAQUS/Standard 2017 are adapted to simulate the behavior of curved steel-concrete composite beam, taking into account geometry and materials nonlinearities. The load-deflection curves and crack patterns have been used to validate the FE results with the results of specimens experimentally tested by Tan and Uy (2009). After the results of the FEM become in acceptable limits with the experimental test, the model is used for a parametric study for some parameters to know the effect of these variables on curved composite beams behavior. The curvature of curved composite beam, the compressive strength of concrete slab, the transverse web stiffeners, the shear connector ratio, and the yield stress of steel beam are investigateded in this parametric study. The test specimen geometry detailed, contact condition, material behavior, element type, and the solution technique are explained in the following sections.

3.1 Material Modelling

In uniaxial tension, the experimental test shows that structural steel behavior reveals strain hardening behavior rather than elastic-perfect-plastic behavior, Byfield et al. (2002). Using strain hardening in the stress-strain curve in the nonlinear analysis has shown well demeanor, Liang et al. (2000, 2004). In the finite element model, the behavior of the reinforcement bars, the steel beam and stud shear connectors are similar using a bilinear stress-strain curve, representing elastic-plastic material with strain hardening. ABAQUS for this demand requires input data of Young's modulus (E_s), Poisson's ratio (v), to represent the elastic behaviour, the yield stress (f_y), the ultimate tensile strength of steel (f_u) and the corresponding inelastic strains for the purpose of defining the plasticity behavior. Assuming identical tension and compression behavior a typical stress-strain relationship for steel is shown in Figure 2.

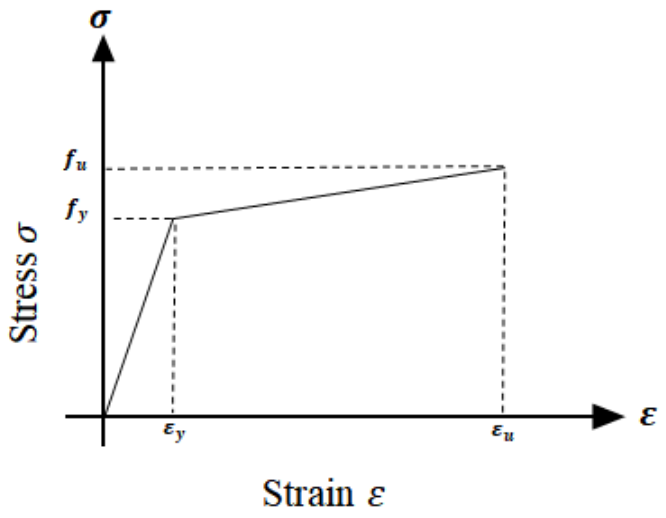

Figure 2. Uniaxial stress–strain relationship of the steel material

International Journal of Mathematical, Engineering and Management Sciences
Vol. 5, No. 6, 1210-1233, 2020
https://doi.org/10.33889/IJMEMS.2020.5.6.091

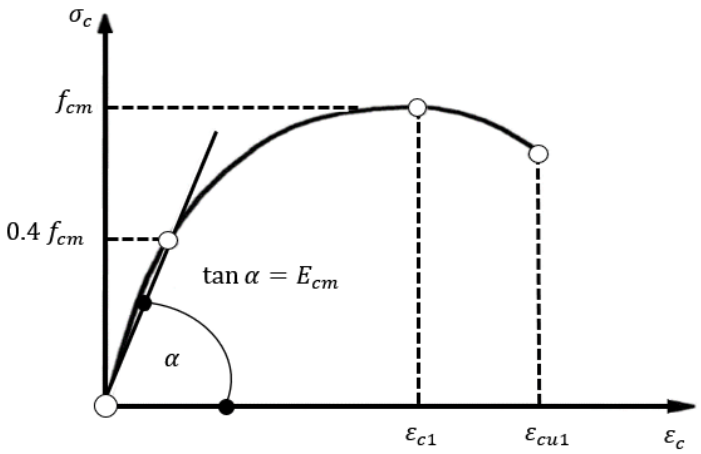

Figure 3. Schematic the stress–strain representation of the concrete material, Eurocode 2 (2004)

The concrete damage plasticity model (CDP) is selected to describe the concrete slab behavior in the curved composite beam in this paper. The presented model is capable of modeling reinforced concrete structures and also designed for application in which the concrete is subjected to monotoning loading under low confining pressure, Hibbit et al. (2012a). In this model, two failure mechanisms are assumed, i.e., tensile cracking and compressive crushing. The control mechanism of yield surface was achieved by two hardening variables associated with the tensile and compression failure mechanisms, respectively. The elastic properties of the concrete are specified by the modulus of elasticity to be secant in the range of $(0 - 0.4\ f_{cm})$ as in equation 1 and the Possion's ratio (v) of 0.2 according to Eurocode 2 (2004). The modulus of elasticity of concrete (E_{cm}) was calculated using prescribed relation in Eurocode 2 (2004),

$$E_{cm} = 22000\ \left[\frac{f_{cm}}{10}\right]^{0.3} \tag{1}$$

$$f_{cm} = f_{ck} + 8 \tag{2}$$

Where, f_{cm} is the cylinder concrete compressive strength (mean value) and f_{ck} is the characteristic cylinder concrete compressive strength at 28 days. Compression and tension behavior in the form of plasticity and damage coefficient are required to create the FE model. In the uniaxial compression of concrete, the hardening region was determined using Eurocode 2 (2004), as described in equation 3,

$$\sigma_c = f_{cm}\ \left[\frac{k\eta - \eta^2}{1 + (k-2)\eta}\right] \tag{3}$$

where,

$$\eta = \frac{\varepsilon_c}{\varepsilon_{c1}} \tag{4}$$

International Journal of Mathematical, Engineering and Management Sciences
Vol. 5, No. 6, 1210-1233, 2020
https://doi.org/10.33889/IJMEMS.2020.5.6.091

and

$$k = \frac{1.05\ E_{cm}|\varepsilon_{c1}|}{f_{cm}} \tag{5}$$

σ_c is the concrete compressive strength for $0 < |\varepsilon_c| < \varepsilon_{cu1}$, ε_c is the concrete compressive strain, ε_{c1} is the compressive strain of concrete at peak stress f_{cm}, and ε_{cu1} is the ultimate compressive strain in the concrete. The Eurocode 2 (2004) specified that the ultimate strain for characteristic compressive strength of concrete between 12-50 MPa, can be taken as 0.0035. For ε_{c1}, Majewski proposed approximating formula (high accuracy) to calculate ε_{c1} depending on the experimental result from the following expression:

$$\varepsilon_{c1} = 0.0014\ (2 - e^{-0.024 f_{cm}} - e^{-0.14 f_{cm}}) \tag{6}$$

The schematic representation of nonlinear structural analysis for the stress-strain relationship of concrete in compression is shown in Figure 3.
whilst concrete tensile behavior, the tensile stresses are assumed to vary linearly with the increase in concrete tensile strain until cracking of the concrete, this hypothesis is applied to the continuation of the analysis process. However, the tensile stress calculated according to Eurocode 2 (2004) is described in equation 7:

$$\sigma_t = f_{ctm}\ \left(\frac{\varepsilon_t}{\varepsilon}\right)^{0.4} \tag{7}$$

Here, f_{ctm} is the concrete tensile strength, which is expressed by the following relationship as in Eurocode 2 (2004):

$$f_{ctm} = 0.3\ (f_{ck})^{\frac{2}{3}} \tag{8}$$

The stiffness degradations coefficients for the concrete damaged plasticity material model for compression (d_c) and tension (d_t) are another important parameter in the damage plasticity model available in ABAQUS. They describe the evolution of the concrete stresses when the concrete material reaches peak stress. Numerous methods are available to achieve the damage parameter. Nguyen and Kim (2009) presented the following relations for defining prescribed parameters, $d_c = 1 - \frac{\sigma_c}{f_{cm}}$ and $d_t = 1 - \frac{\sigma_t}{f_{ctm}}$ for compression and tension, respectively. The properties of the materials used in curved composite beams are provided in Table 2.

International Journal of Mathematical, Engineering and Management Sciences
Vol. 5, No. 6, 1210-1233, 2020
https://doi.org/10.33889/IJMEMS.2020.5.6.091

Table 2. Material properties of the composite beam curved in plan beams.

Material	Material property (MPa)	CCBP-1	CCBP-2	CCBP-3
Concrete	Compressive strength f_{cm}	37.7	39.1	40.4
Steel web	Yield strength f_y	374		
	Ultimate strength f_u	512		
Steel flange	Yield strength f_y	347		
	Ultimate strength f_u	495		
Steel stirrups	Yield strength f_y	399		
	Ultimate strength f_u	498		
Steel reinforcement	Yield strength f_y	586		
	Ultimate strength f_u	683		
Stud shear connector	Yield strength f_y	395		
	Ultimate strength f_u	499		

3.2 Analysis Technique

In steel-concrete composite curved beams, the concrete slab reveals high discontinuity due to the concrete cracking. To avoid this discontinuity in the solution, the modified Riks method often utilized to predict nonlinear collapse with beam softening (ABAQUS Users Manual 2016). Riks method is capable to deal with complicated behavior of the material, geometric nonlinearities, and contact problem. Moreover, the main benefit of employing this method is to conduct the high demeanor of the nonlinear distortion, as obtained in the laboratory experiments of the composite steel-concrete beam, Abaqus (2009).

3.3 Element Type and Interaction Condition

Figure 4 shows the model components, the mesh and the type of elements used in the finite element model for curved composite steel-concrete beams. The beam consisting of four parts: the concrete slab, shear connectors, reinforcement bars, and steel beam. Solid element (C3D8R) is utilized to simulate the reinforced concrete slab, shear connectors, web stiffeners, and the steel beam. This element is a three-dimensional eight-noded that has three degrees of freedom at each node, reduced integration with hourglass control with a linear approximation of displacement. The stresses at every integration point have been provided at several points through the thickness. Truss element (T3D2) is adaptive to simulate the reinforcement steel bars. T3D2 is a three-dimensional element with a linear approximation of displacement, two nodes and three translations of displacement in *x*,*y* and *z* directions. Constant stresses are assumed through the element, where the moment or forces perpendicular to the centerline for truss element are eliminated, Hibbitt et al. (2012b).

Once all parts are assembled at an appropriate location, a proper constraint used to describe the interaction between components as presented in Figure 5. In the FE model, different parts interact using the constraint and interaction option in ABAQUS. Three types of interaction are presented in the current paper. The first chosen type is surface to surface contact available in ABAQUS, utilized here for interface contact between the steel beam and the concrete slab. The upper surface of the steel beam flange connects to the bottom surface of a concrete slab at the position of contact with the steel beam. The concrete surface has been chosen to be the master surface whilst the upper steel beam flange to be a slave surface. The second chosen type is a tie constraint utilized to describe the contact behavior between the shear connector and the steel beam flange as well as the welding simulation of the transverse stiffeners to the steel beam. This type of interaction is employed to eliminate the slip between the two contact surfaces, where each node at the stud shear connector and the transverse stiffener surfaces have the same rotational motions and translation as well as the

International Journal of Mathematical, Engineering and Management Sciences
Vol. 5, No. 6, 1210-1233, 2020
https://doi.org/10.33889/IJMEMS.2020.5.6.091

node on the contact surfaces of the steel beam. Finally, the embedded constraint is utilized to constrain the reinforcement bar nodes to a relative degree of freedom of the concrete slab which is considered as the host element. Furthermore, it is employed to represent the shear stud connector within the concrete slab by considering the top surfaces of each shear connector to be embedded inside the concrete.

3.4 Boundary and Loading Conditions

The experimental specimens are designed as simply supported in flexure whereas the concrete slab was being restrained at both ends against twisting. In order to simulate the test specimen, one end of the bottom steel flange of the FE model was prevented from translation in x, y and z directions while the other end restrained in x and y directions. To properly simulate the twisting boundary conditions, both ends of the concrete slab are restrained against translation displacement at x and y directions. Loading was applied as a displacement control, where the displacement is applied downward as pressure forces to avoid the high stress concentration on the concrete slab. Prescribed boundary conditions are summarized in Figure 6.

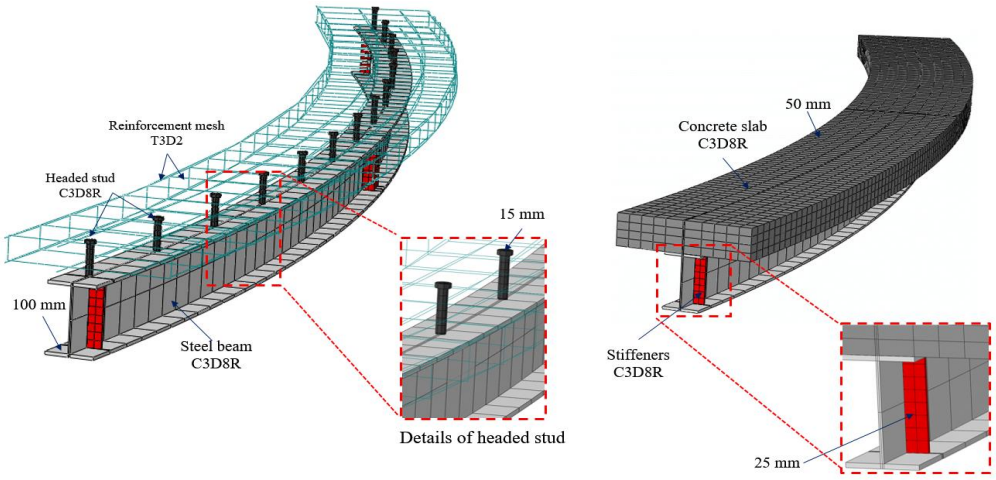

Figure 4. The model of the beam in the ABAQUS program

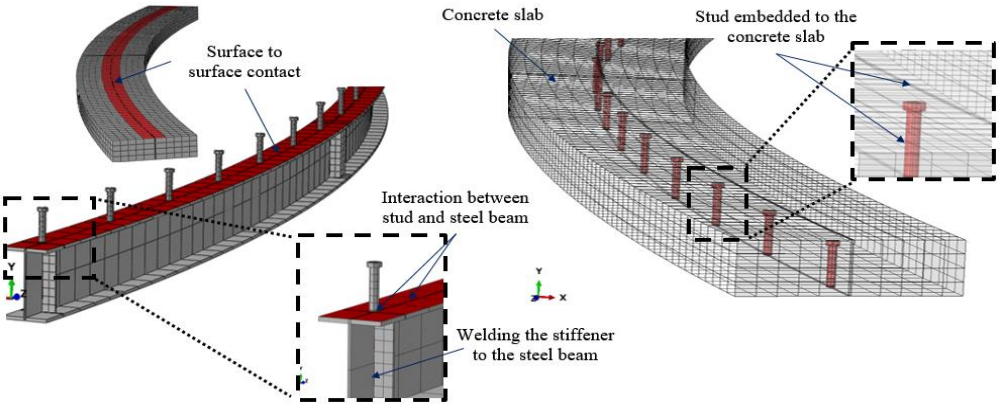

Figure 5. Interaction and the constraint condition in the model

International Journal of Mathematical, Engineering and Management Sciences
Vol. 5, No. 6, 1210-1233, 2020
https://doi.org/10.33889/IJMEMS.2020.5.6.091

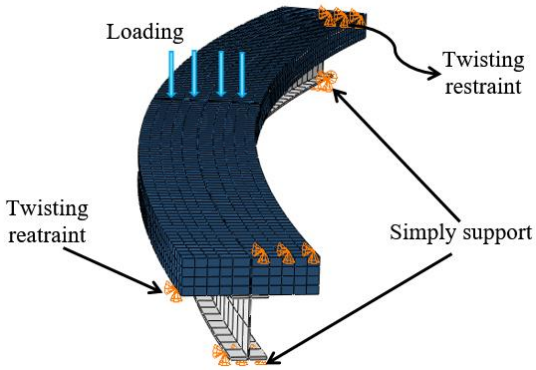

Figure 6. Boundary and applied loading conditions for the finite element modeling

4. Comparison with Experimental Results

The load-deflection relationship for the numerical and the experimental test results of CCBP-1 specimen is demonstrated in Figure 7a. The finite element results showed excellent agreement with the experimental results. The ultimate loads are 122 kN and 122.02 kN for the model and the tested beam, respectively. The stiffness, strength and ductility are identical for both experiment and FE during each loading stage. Figure 7b shows the load-defection behavior of the test and the FE model for specimen CCBP-2. The stiffness of both specimens is in a close agreement up to a load of 40 kN. Beyond this load value, the specimen follows a similar variation in stiffness wherein a sudden drop in the load is recorded for the tested beam at a load of 114 kN. The FE and experimental results are in good agreement in terms of ultimate load and deflection at failure load, while a small difference in deflection values in the ultimate stage is found, Table 3. The difference in the load-deflection curve could be due to the applied loading condition, where the experimental beams is loaded under loading control. For specimen CCBP-3 the finite elment results related to the load-deflection curve are demonstrated in Figure 7c. It shows that the results are in a good agreement with the test ones. An ultimate load of 83.71 kN has been recorded in the numerical model which is acceptable comparing to 78 kN obtained in test. Figure 8 shows the development of the diagonal torsional cracks of concrete slab for CCBP-2 specimen at the top surface of one end. As it is clear the diagonal cracks in the numerical models appear to expand more than the experimental results. This could be due to the stress concentration of the loads on the top surface of the slab by displacement control.

International Journal of Mathematical, Engineering and Management Sciences
Vol. 5, No. 6, 1210-1233, 2020
https://doi.org/10.33889/IJMEMS.2020.5.6.091

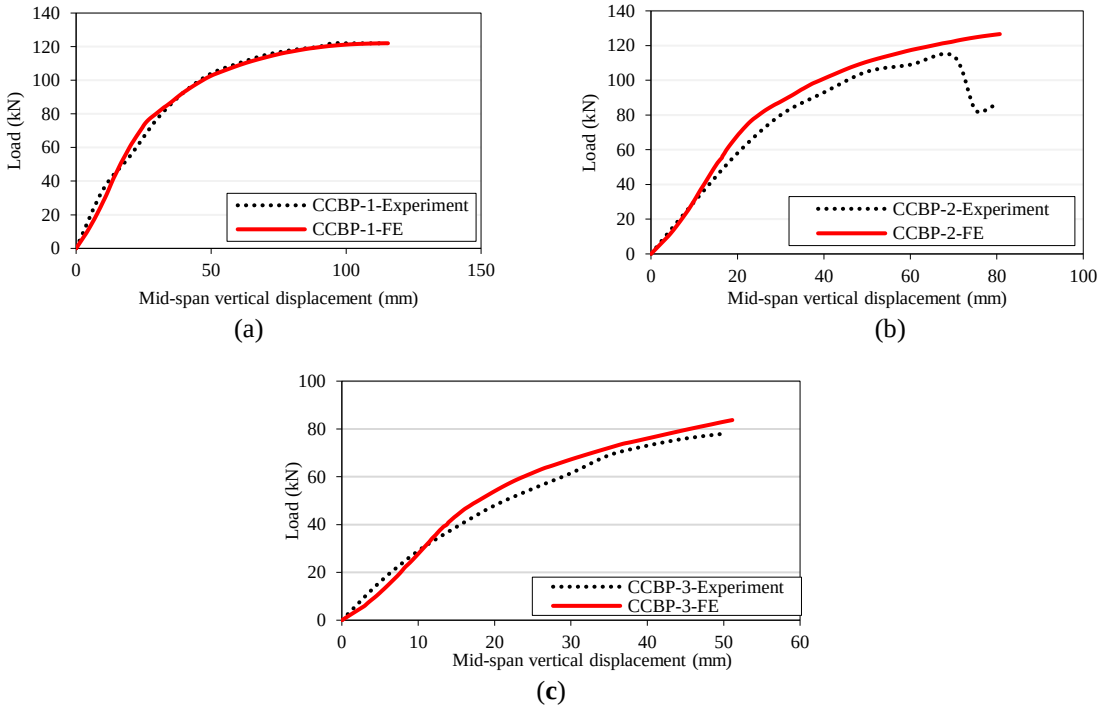

Figure 7. Comparison of the theoretical and experimental load-displacement: (a) Specimen CCBP-1; (b) Specimen CCBP-2; (c) Specimen CCBP-3

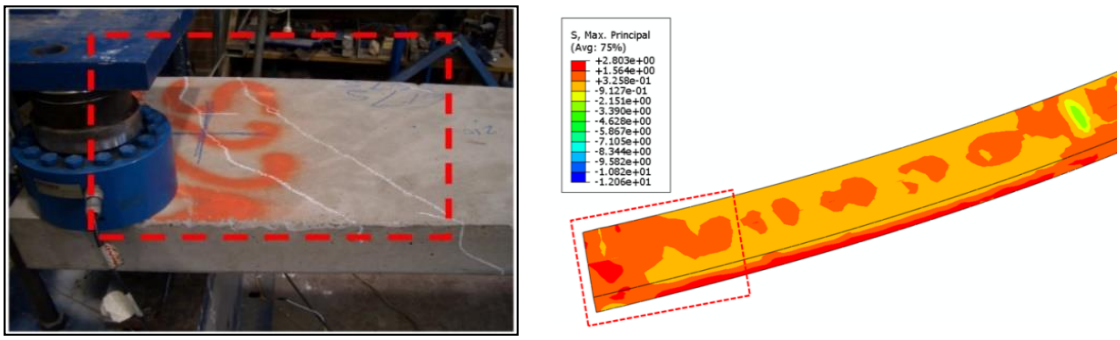

Figure 8. Maximum principle stress contour for CCBP-2

Table 3. Comparison between the numerical and experimental results.

Specimen No.	Span/Radius	P_u(kN)		$\frac{P_{EXP}}{P_{FEA}}$	Δ_u(mm)		$\frac{\Delta_{Exp}}{\Delta_{FEA}}$	Δ_{uf}(mm)		$\frac{\Delta_{uf\ EXP}}{\Delta_{uf\ FEA}}$
		P_{EXP}	P_{FEA}		Δ_{EXP}	Δ_{FEA}		$\Delta_{uf\ EXP}$	$\Delta_{uf\ FEA}$	
CCBP-1	0.275	122	122.02	0.99	115	115.51	0.99	121	120.96	1.00
CCBP-2	0.294	114	126.64	0.90	68	80.69	0.84	79	80.69	0.98
CCBP-3	0.455	78	83.71	0.93	47	51.13	0.92	49	51.13	0.96

P_u , Δ_u and Δ_{uf} :the ultimate load, deflection at ultimate load and the deflection at failure, respectively.

International Journal of Mathematical, Engineering and Management Sciences
Vol. 5, No. 6, 1210-1233, 2020
https://doi.org/10.33889/IJMEMS.2020.5.6.091

5. Parametric Study

The essential objective of the presented paper is to investigate the effect of several important parameters that are not been well covered in past the previous studies on the inelastic behavior, crack patterns, ductility, stiffness and strength of curved composite steel–concrete beams. The span/radius of curvature ratio, transverse web stiffeners, partial interaction, concrete compressive strength and steel beam yield stress are the considered parameters in this study, Figure 9. The finite element modeling is carried out and developed using the general commercial ABAQUS software. The parametric study results obtained from the finite element analysis including the yield load (P_y), ultimate failure load (P_u) and the ultimate vertical mid-span deflection (Δ_u). The curve beam strength and the load versus mid-span deflection relation are included in each parameter involved to focuses on the effect of these variables on all the numerical models.

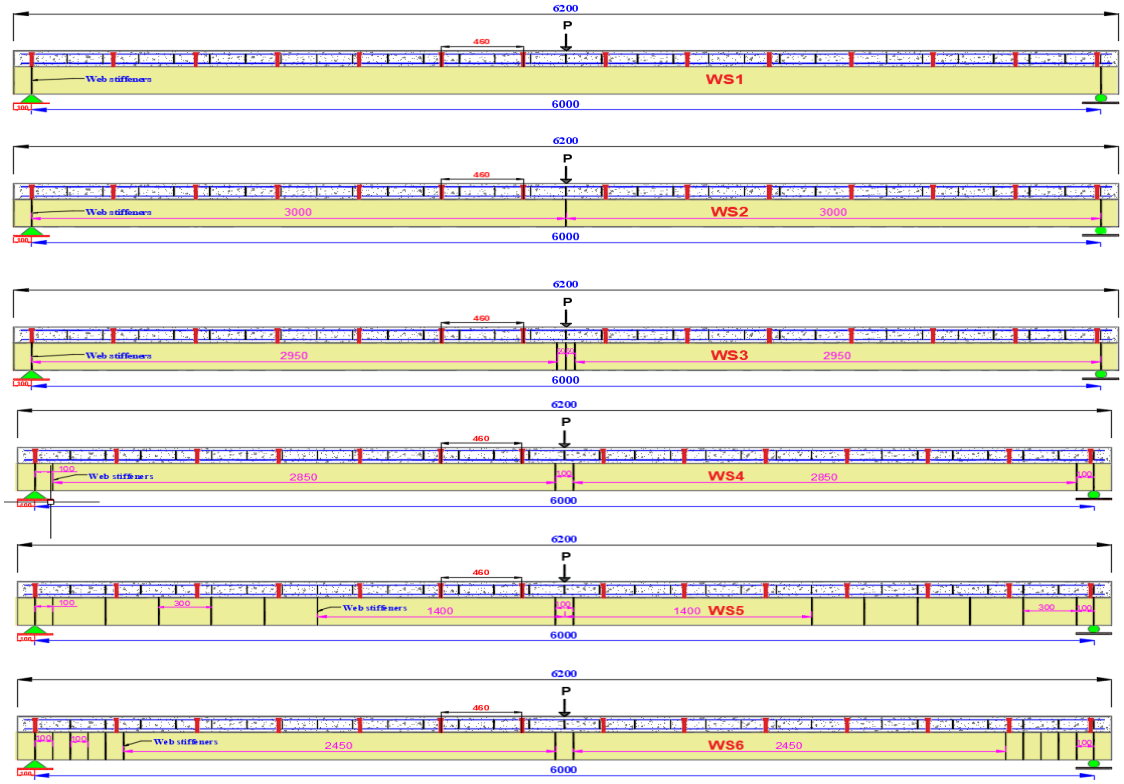

Figure 9. Geometry and dimensions of the curved composite beam with web stiffeners (unit: mm)

5.1 Effect of Span/Radius of Curvature Ratio

The validated model CCBP-1 was contrived to investigate the effect of the span/radius ($\frac{L}{R}$) of curvature ratio on the inelastic behavior of the curved composite beam. The numerical models had the same span length, material properties and loading conditions as beam CCBP-1, presented in a previous study by Tan and Uy (2009), but with various angles. Figures 10 and 11 show the load versus deflection and the load versus central angle relations of the beams undergo for different span/radius of curvature effect. In these Figures A-10, A-20, A-30 and A-40 represent the beams with central angles ($\theta = 10^{\circ}$,20°, $30^{\circ}$and 40°), respectively. Based on the obtained results, it can

International Journal of Mathematical, Engineering and Management Sciences
Vol. 5, No. 6, 1210-1233, 2020
https://doi.org/10.33889/IJMEMS.2020.5.6.091

be noted that the beam began to yield at an early stage when the span/radius ratio increases, and inelastic behavior developed early, as seen in Table 4. Compared to the specimen A-10, the other three specimens recorded a reduction in yield load by 13%, 21% and 39.5% for A-20, A-30 and A-40, respectively. In the case of load-carrying capacity, the ultimate load of composite beams seems to reduce in a range of 13%, 25% and 42.7% for A-20, A-30 and A-40, respectively, compared to A-10. The numerical ultimate vertical deflection decreases by 16.33%, 24% and 44.5% for a specimen for A-20, A-30 and A-40, respectively compared to A-10.

Furthermore, it can be noted from the load versus mid-span deflection curves in Figure 10 that all the numerical curves appear to reduce the ductility of composite beams significantly with the increasing of central angle. These leads to the conclusion that the response of the specimens softens, and the yielding of the beams get earlier. From Figure 12, it is evident that when the ratio increasing, the vertical separation between the concrete slab and steel beam flange at the beam mid-span and the twisting at the mid-section increase and be more evident. This observation in the twisting and the vertical separation may be attributed to the effect of torsion as the ratio increases and failure of the beam change from flexure to a combined effect of flexural and torsional. Moreover, the torsion is found to be a dominant and influential on the inelastic behavior and failure mechanism of the beam, especially in specimens with larger span/raids of curvature ratio, A-30 and A-40. Figure 12 also shows the flexural crack patterns of the curved beams in which the tension zone is found to be firstly initiated in the central zone then widened and propagated toward the whole slab when the ratio increased. The observed increase in the cracks was due to the increase in shear stresses in the specimens when the ratio increases due to an increase in the torsional effect. The cracks in the compression face are observed to be little compared with the tension face.

Table 4. Parameters for studying the effect of Span/radius of curvature ratio (L/*R*) on the curved composite beam.

Beam type	**Specimen (A_i)**	**Central angle (°)**	**Span/Radius**	**Curve composite beam behavior**					
				F_{yA-i} **(kN)**	F_{uA-i} **(kN)**	Δ_u **(mm)**	$\frac{F_{yA-i}}{F_{yA-10}}$	$\frac{F_{uA-i}}{F_{uA-10}}$	$\frac{\Delta_{uA-i}}{\Delta_{uA-10}}$
CCBP-2	A-10	10	0.175	107.5	138.8	146.3	1.00	1.00	1.00
	A-20	20	0.349	93.5	120.7	122.4	0.87	0.87	0.84
	A-30	30	0.524	85.04	104.6	111.1	0.79	0.75	0.76
	A-40	40	0.698	65.05	79.44	80.94	0.61	0.57	0.55

F_{yA_i}: Yield load of the specimens $\mathbf{A_i}$.; $F_{yA_{10}}$: Yield load of specimens $\mathbf{A_{10}}$.

International Journal of Mathematical, Engineering and Management Sciences
Vol. 5, No. 6, 1210-1233, 2020
https://doi.org/10.33889/IJMEMS.2020.5.6.091

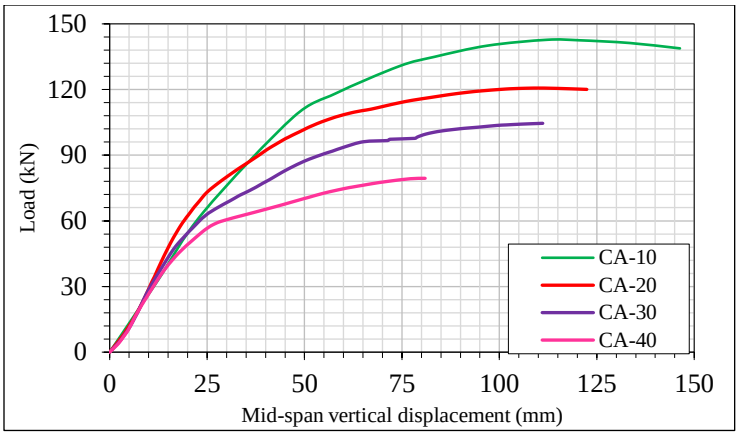

Figure 10. Span/radius of ratio effect on the load-deflection curve of the curve composite

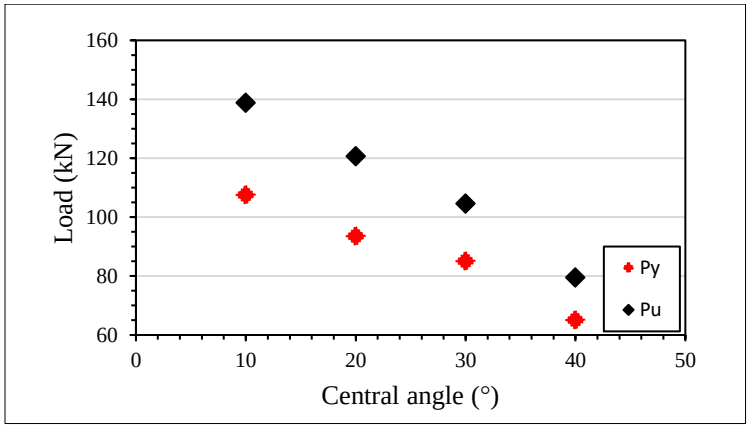

Figure 11. Yield, ultimate load-central angle relationship

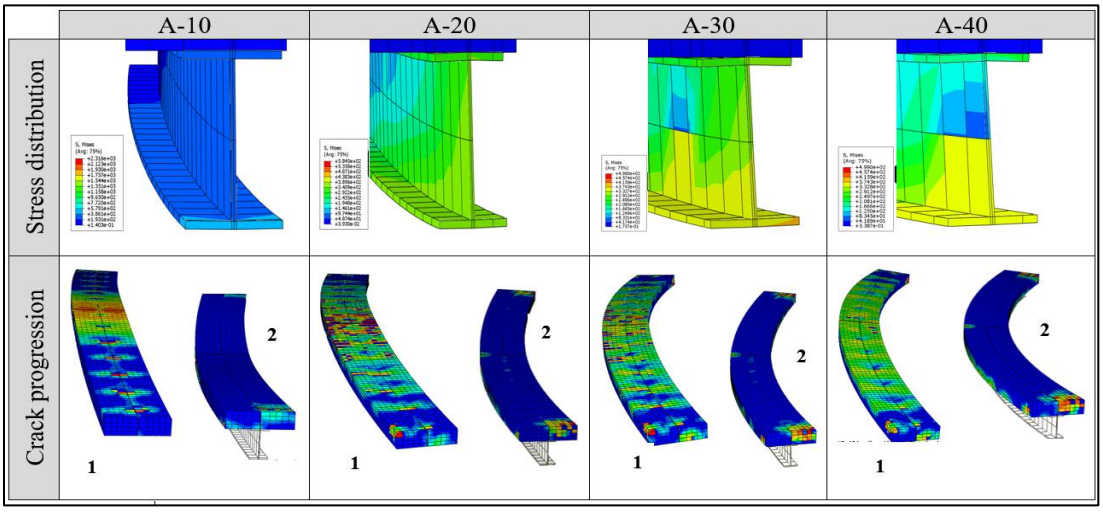

Figure 12. Effect of span/radius ratio on: (a) Stress distribution; (b) Crack progression on the slab, 1- Top surface of the beam, 2- Bottom surface of the concrete slab

International Journal of Mathematical, Engineering and Management Sciences
Vol. 5, No. 6, 1210-1233, 2020
https://doi.org/10.33889/IJMEMS.2020.5.6.091

5.2 Transverse Web Stiffeners' Effect

In order to illustrate the vertical web stiffeners' effect on the inelastic behavior and the performance of the curved composite steel–concrete beams, a group of beams with different numbers and locations of web stiffeners was analysed using the numerical method as seen in Figure 9. The web stiffners with nominal thickness of 6.5 mm are arranged in the validated model CCBP-3, as shown in Figure 1. The numerical models have the same span length, material properties and loading conditions as in the beam CCBP-3, presented in a previous study of Tan and Uy (2009). Figures 13 and 14 show the comparison of the load versus mid-span defletion and load relasions of the curved beams with different arrangement of transverse stiffeners. Based on the obtained results, the presence of web stiffeners at different locations in the curved composite beam affected the shear strength capacity. Specimens WS-2 and WS-3 showed a slight reduction in the beam deflection accompanied with increases in the beam capacity to 4.5% and 8% for WS-2 and WS-3 respectively, if compared to the WS-1 model.

Specimens with transverse stiffeners near to the supports show increase in the shear strength capacity by 22.8%, 27.55% and 34.43% for specimens WS-4, WS-5 and WS-6 respectively, compared with WS1, as depicted in Figure 12. The specimens WS-5 and WS-6 recorded an increase in beam deflection by 9% and 42% compared to WS-1, respectively. The observed variance in these values is due to the stiffeners' locations. It can be observed that the beams begin to yield at an early stage as the stiffener number increases, as it is clear in Table 5. The web twisting and vertical separation between the concrete slab and steel beam flange at the beam mid-span, which is an important issue, are observed to decrease as the number of stiffeners increases in this zone, as shown in Figure 15, especially in WS-3. This reduction in the twisting and vertical slip may be attributed to decrease the beam torsion incorporating with transferring the failure of the composite beam from steel beam to the concrete slab. Moreover, the existence of the stiffeners with different locations redistributed the crack progression in the slab and presented more compression and flexural cracks in the slab center span as demonstrated in Figure 15. Furthermore, the stiffners do not affect the interface slip between the steel beam flange and the reinforced concrete slab. However, the effect of the the transvers web stiffeners should be taken into account in the analysis of the curved composite beam.

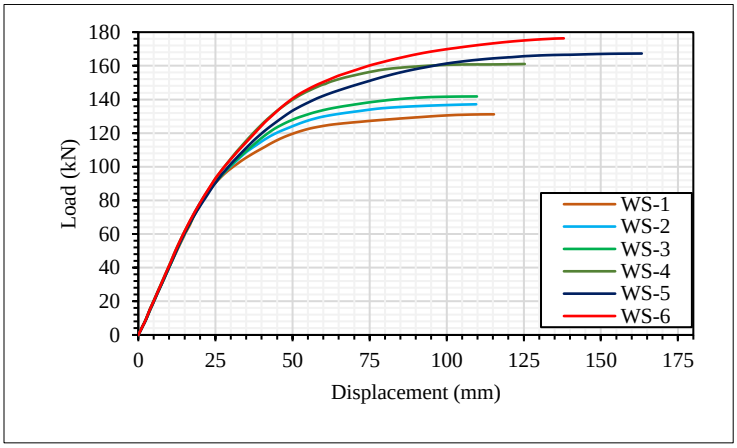

Figure 13. Web stiffener's effect on the load-deflection curve of the curve composite

International Journal of Mathematical, Engineering and Management Sciences
Vol. 5, No. 6, 1210-1233, 2020
https://doi.org/10.33889/IJMEMS.2020.5.6.091

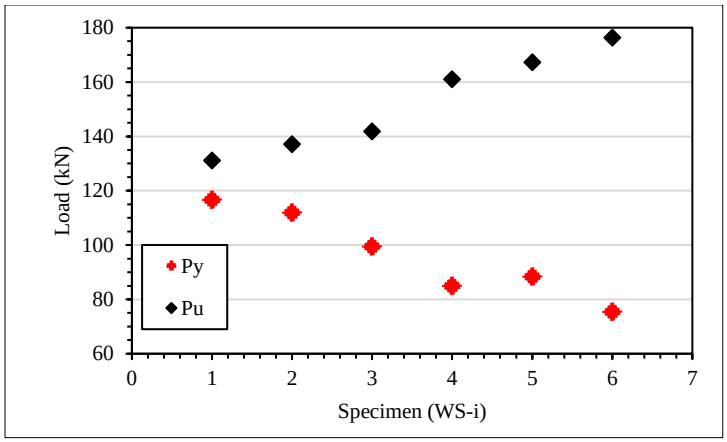

Figure 14. Yield, ultimate load-specimens relationship

Table 5. Web stiffeners effect on the curved composite beam.

Beam type	Specimen (WS-i)	Central angle (°)	Curved composite beam behavior					
			F_{yWS-i} (kN)	F_{uWS-i} (kN)	Δ_u (mm)	$\frac{F_{yWS-i}}{F_{yWS-1}}$	$\frac{F_{uWS-i}}{F_{uWS-1}}$	$\frac{\Delta_{uWS-i}}{\Delta_{uWS-1}}$
CCBP-3	WS-1	26.04	116.60	131.17	115.32	1.00	1.00	1.00
	WS-2		111.28	137.12	109.57	0.95	1.05	0.95
	WS-3		99.38	141.79	109.80	0.85	1.08	0.95
	WS-4		84.97	161.08	125.32	0.73	1.23	1.09
	WS-5		88.31	167.30	163.27	0.76	1.28	1.42
	WS-6		75.43	176.33	137.98	0.65	1.34	1.20

F_{yWS-i}: Yield load of specimens **WS-I**; .F_{yWS-1}: Yield load of specimens **WS-1**.

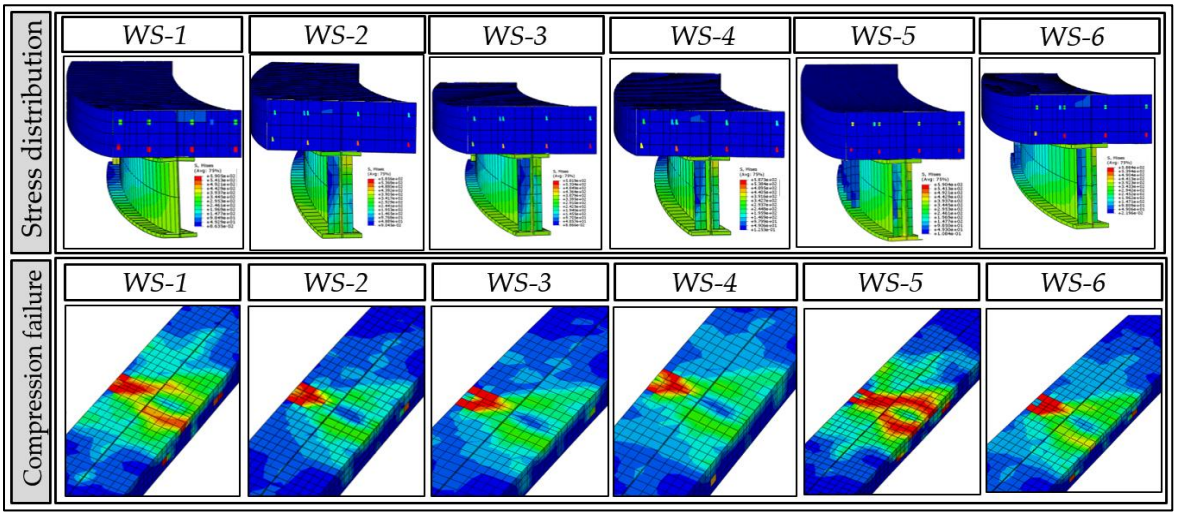

Figure 15. Shear connector effect on the interface separation and the concrete slab compression failure

International Journal of Mathematical, Engineering and Management Sciences
Vol. 5, No. 6, 1210-1233, 2020
https://doi.org/10.33889/IJMEMS.2020.5.6.091

5.3 The Partial Interaction Effect

In this section, the effect of partial interaction or shear connector ratio on the beam capacity of the composite curved beams is studied by considering different ratios of the shear connector of (0.25, 0.3, 0.4, 0.5, 0.65, 0.7, 0.8 0.9 and 1) by changing the connector quantity in the beam. The examined beams ST_8, ST_{10}, ST_{12}, ST_{16}, ST_{20}, ST_{22}, ST_{24}, ST_{26} and ST_{30} represent beams with a number of studs of (8, 10, 12, 16, 20, 22, 24, 26 and 30), respectively. The specimen CCBP-2, which has fourteen stud shear connectors, is used in this comparison. Studs with nominal diameter of 19 mm are arranged as in CCBP-2 specimen in a single row. The beam span length, section properties and the loading condition are the same as in the previous study of Tan and Uy (2009). Figures 16 and 17 show the load versus vertical deflection and the load versus No. of studs relations of beams. Based on the available data, a decease in the ductility of the beam has been noticed as the partial interaction ratio increases, however this is accompanied with an increase in load capacity of the beams. The increases, compared with ST_8, range from (2-29)% for specimens ST_{10} to ST_{30}, respectively as can be seen in Table 6. Models ST_{24}, ST_{26} and ST_{30} show a closer enhancing in the beam capacity by 25, 26 and 30% comparing with specimen ST_8. The deflection along the beam is recorded at 100 kN loading for all specimens as depicted in Figure 18. Obviously, the deflection profile of specimens shows improvement in the serviceability performance of the curved composite members as the stud number increases. Specimens ST_{24}, ST_{26} and ST_{30} show almost a very closer reduction in the deflection value by about 65% compared to ST_8. The observed increasing in the ultimate load can be attributed to full interaction between beam components of the beams when the stud number is increased. It is found that the slip decreases with increasing the partial interaction ratio. The interface slips of the specimens ST_{24}, ST_{26} and ST_{30} is approximately the same, so it is possible to consider them as a case of the beam with full interaction comparing with the remaining beams which are of partial interaction. Moreover, the distribution of flexural cracks in the tension region of concrete slab is found to be lowered as the stud number increases, where the cracks in the lower slab surface gradually decrease to include the lower middle area of a concrete slab under loading surface and the stud area. Additional cracks are observed in the concrete slab compression face essentially in the centroid zone, in which the slab causing compresion mode failure.Thus the effect of the partial interaction should be taken into account for the analysis accuracy. The strength and the stud shear connector stiiffness should be considered in the inelastic analysis of steel-concrete curved composite beam in which the full interaction assumption may overestimate the ultimate strength and underestimate the beam deflection.

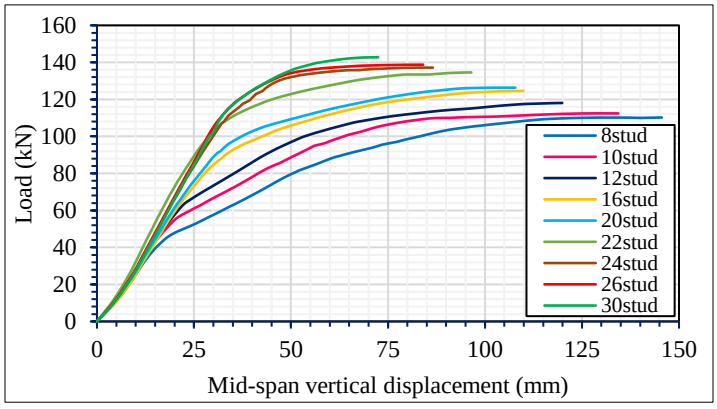

Figure 16. Partial interaction effect on the load-deflection relationship of the curved composite beam

International Journal of Mathematical, Engineering and Management Sciences
Vol. 5, No. 6, 1210-1233, 2020
https://doi.org/10.33889/IJMEMS.2020.5.6.091

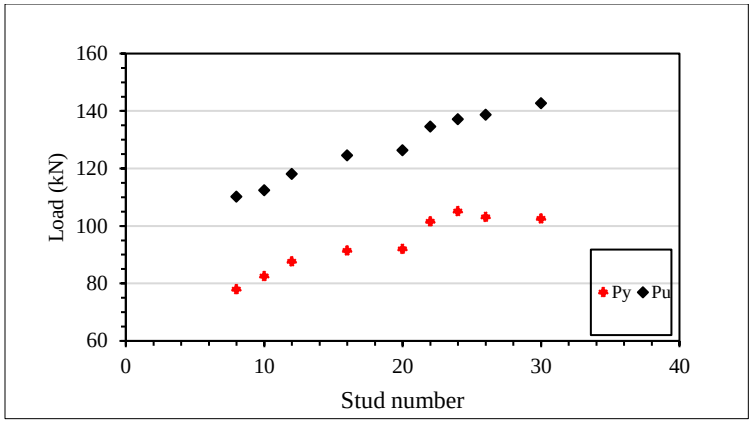

Figure 17. Yield, ultimate load-specimens relationship

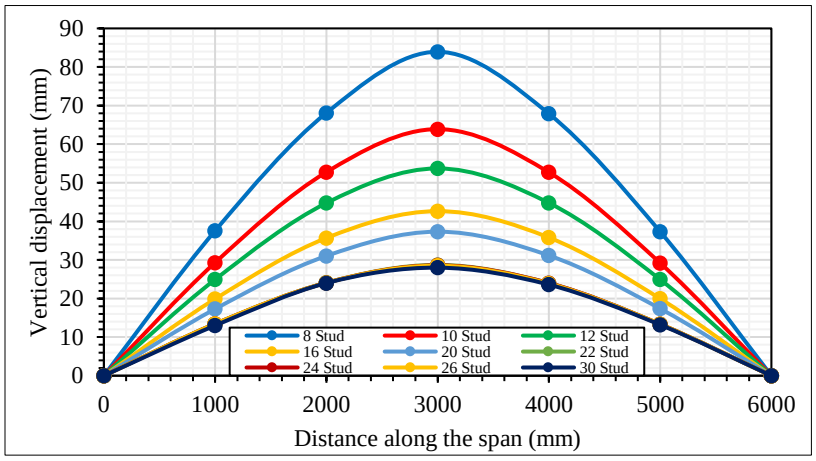

Figure 18. Deflection profile for the curved composite beam at 100 kN loading level

Table 6. Partial interaction effect on the curved composite beam

Beam type	Specimen (ST_i)	Partial interaction ratio (β)	Number of shear connectors	Central angle (°)	Curve composite beam behavior					
					F_{yST_i} (kN)	F_{uST_i} (kN)	Δ_u (mm)	$\frac{F_{yST_i}}{F_{yST_8}}$	$\frac{F_{uST_i}}{F_{uST_8}}$	$\frac{\Delta_{uST_i}}{\Delta_{uST_8}}$
CCBP-2	ST_{30}	1.00	30	16.85	102.58	142.77	72.47	1.32	1.30	0.50
	ST_{26}	0.9	26		103.09	138.74	84.05	1.32	1.25	0.58
	ST_{24}	0.8	24		105.09	137.17	86.57	1.35	1.24	0.59
	ST_{22}	0.7	22		101.49	134.17	96.47	1.30	1.22	0.66
	ST_{20}	0.65	20		91.94	126.34	107.83	1.18	1.15	0.74
	ST_{16}	0.5	16		91.34	124.60	109.91	1.17	1.13	0.76
	ST_{12}	0.4	12		87.63	118.07	119.91	1.12	1.07	0.82
	ST_{10}	0.3	10		82.45	112.42	134.37	1.06	1.02	0.92
	ST_8	0.25	8		77.92	110.18	145.55	1.00	1.00	1.00

F_{yST_i}: Yield load of specimens **ST_i.;** $F_{yST_{30}}$: Yield load of specimens **ST_{30}.**

International Journal of Mathematical, Engineering and Management Sciences
Vol. 5, No. 6, 1210-1233, 2020
https://doi.org/10.33889/IJMEMS.2020.5.6.091

5.4 The Concrete Slab's Compressive Strength Effect

The effect of the concrete slab compressive strength is introduced using various values for concrete grades of C22, C32, C42. These values represent the concrete compressive strength values in most design standards for normal weight concrete. The analysis is performed on the specimen A-30 (with 30◦ an included angle) at which the section geometry and the properties of the material are identical with the specimen used in the current study exccept the concrete compressive strength, to investigate their performance and effect on the inelastic behavior of the composite beam curved in plan. The properties of concrete material including the characteristic compressive strength f_{ck}, the mean value of compressive and the tensile strength f_{cm} and f_{ctm}, respectively, and the modulus of elasticity E_{cm} are in accordance to Eurocode 2 (2004), Table 7. Figuress 19 and 20 show the load versus deflection and the load versus concrete compressive strength of the beams. In these Figures, C_{30}, C_{40} and C_{50} represent the beams with concrete compressive strength of (30, 40 and 50) MPa, respectively. It can be seen that the specimen C_{30} exhibits more ductility comparing with the remaining two beams. Moreover, the load carrying capacity increases by about 15.86 % and 34.4% for specimens C_{40} and C_{50} compared with C_{30}, respectively, however the increase in yielding load is less of approximately 8.4%, Table 8. The predicted ultimate vertical deflection is less by 8% and 18% for C_{40} and C_{50}, respectively. Concerning the flexural crack patterns, the cracks seem to be less remarkable when compared with the above two parameters. Furthermore, increasing the concrete compressive strength does not affect the vertical and the interface slip between the steel beam flange and the reinforced concrete slab.

Table 7. The concrete slab properties for parametric study.

Concrete properties	**Curved composite beam behavior**		
	C22	**C32**	**C42**
f_{ck} (MPa)	22	32	42
f_{cm} (MPa)	30	40	50
f_{ctm} (MPa)	2.36	3.02	3.79
E_{cm} (GPa)	30.6	33.35	35.65

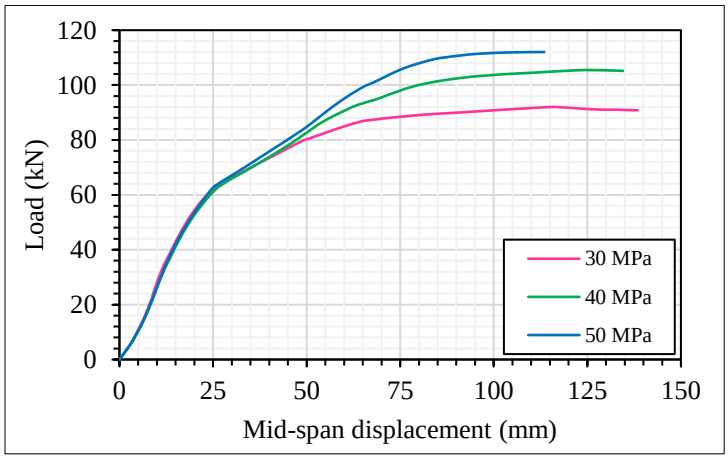

Figure 19. Effect of the compressive strength on the load-deflection curve

International Journal of Mathematical, Engineering and Management Sciences
Vol. 5, No. 6, 1210-1233, 2020
https://doi.org/10.33889/IJMEMS.2020.5.6.091

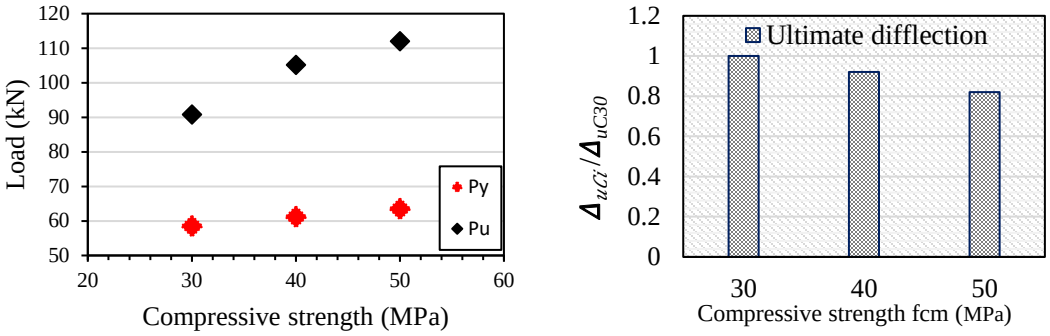

(a) Beam strength (b) Beam deflections

Figure 20. The concrete compressive strength effect on the ultimate strength and the ultimate deflection of the composite curved beam

Table 8. Effect of compressive strength on curve composite beam.

Beam type	Specimen (C_i)	Compressive strength (f_{cm}) MPa	Central angle (°)	Curve composite beam behavior					
				F_{yC_i} (kN)	F_{uC_i} (kN)	Δ_u (mm)	$\frac{F_{yC_i}}{F_{yC_{30}}}$	$\frac{F_{uC_i}}{F_{uC_{30}}}$	$\frac{\Delta_{uC_i}}{\Delta_{uC_{30}}}$
A-30	C_{30}	30	26.04	58.52	90.82	138.45	1.00	1.00	1.00
	C_{40}	40		60.17	105.2	127.37	1.03	1.16	0.92
	C_{50}	50		63.45	112.04	113.48	1.08	1.23	0.82

F_{yC_i}: Yield load of specimens **C_i.,** F_{yC_i}: Yield load of specimens **C_{30}.**

5.5 The Steel Beam Yield Stress Effect

The yield stress of steel beam is considered in the current study to discuss the influence of this parameter on the inelastic behavior and the performance of the curved composite beam. The considered yield stress values for the web and flanges of the steel beam are 200, 250, 300, 350, 400 and 450 MPa. Figures 21 and 22 show the load-deflection and the load-yield stress relations of the curved composite beam. Specimens S_{200}, S_{250}, S_{300}, S_{350}, S_{400} and S_{450} represent the curved composite beams with beam yield stress equal to (200, 250, 300, 350, 400 and 450), respectively. Material behaviour, length of the beam , sectional properties and loading condition are the same as in the previous study of Tan and Uy (2009) for specimen CCBP-2. From the FE analysis, the increase of the steel beam yield stress leads to increase the curved composite beam yield load and also the ultimate load. The percentage increase in ultimate load is 14, 30, 40, 46.5 and 58% compared with S_{200}, as seen in Table 9. The predicted vertical deflections show almost a significant increases in all specimens with a percentage range of 4.7% to 25.5% as can be seen in Table 9. Moreover, the stress distribution of steel beam is found to be changed as the yield stress increase especially in specimen S_{450}. However, the flexural cracks are less or negligible in the bottom and top faces of the reinforced concrete slab comparing with the other parameters. While for the vertical and interface slip, the effect is either negligible or ineffective.

International Journal of Mathematical, Engineering and Management Sciences
Vol. 5, No. 6, 1210-1233, 2020
https://doi.org/10.33889/IJMEMS.2020.5.6.091

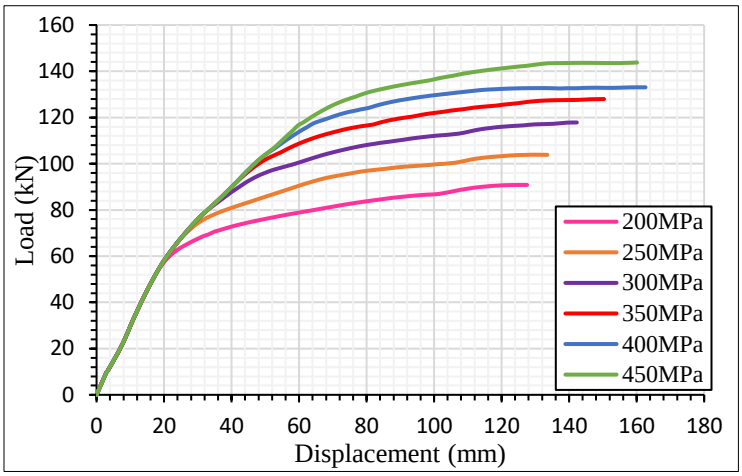

Figure 21. The steel beam yield stress on the load-deflection curve

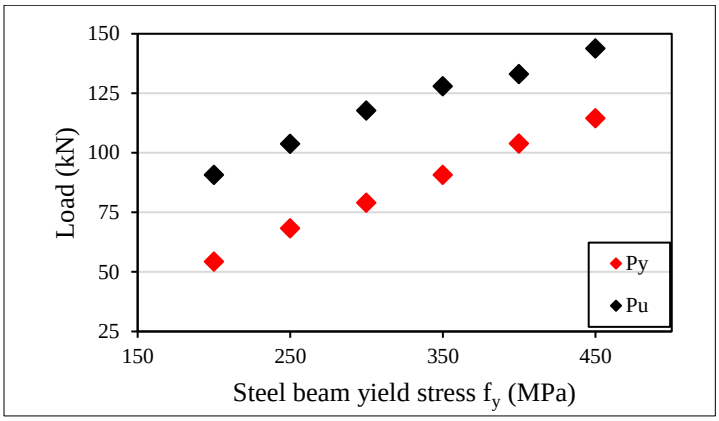

Figure 22. Yield, ultimate load-steel beam yield stress relationship

Table 9. Effect of the yield stress on the curved composite beam.

Beam type	**Specimen (S_i)**	**Central angle (°)**	**Curved composite beam behavior**					
			F_{yS_i} **(kN)**	F_{uS_i} **(kN)**	Δ_u **(mm)**	$\frac{F_{yS_i}}{F_{yS_{200}}}$	$\frac{F_{uS_i}}{F_{uS_{200}}}$	$\frac{\Delta_{uS_i}}{\Delta_{u200}}$
CCBP-2	S_{200}	16.85	54.36	90.82	127.56	1.00	1.00	1.00
	S_{250}		68.28	103.84	133.55	1.26	1.14	1.05
	S_{300}		79.06	117.83	142.83	1.45	1.30	1.12
	S_{350}		90.82	127.97	150.35	1.67	1.41	1.18
	S_{400}		104.0	133.07	162.64	1.91	1.47	1.28
	S_{450}		114.5	143.78	160.10	2.11	1.58	1.26

F_{yS_i}: Yield load of specimens **S_i.,** $F_{yS_{200}}$: Yield load of specimens **S_{200}.**

International Journal of Mathematical, Engineering and Management Sciences
Vol. 5, No. 6, 1210-1233, 2020
https://doi.org/10.33889/IJMEMS.2020.5.6.091

6. Conclusions

Three-dimensional FEM are developed to simulate composite steel–concrete beams curved in plan, as previous studies have failed to study the inelastic behavior of such beams under static loading when changing the various beam properties. The plastic damage and compressive plastic models are used to represent the nonlinear behavior of all parts of the model. The load-deflection curve behavior obtained from FEA was compared with the results of the experimental test to ensure the accuracy of the FE results. A parametric study was conducted using the proposed validated FE models. Based on the obtained theoretical results, the following conclusions can be drawn:

- It was shown that when the span/radius ratio increased, the ultimate capacity of the member decreases, and the flexural cracks patterns increased and expanded along with the concrete slab. Moreover, the beams exhibited less ductility with increases the span/radius ratio, which leads to the conclusion that the response of the specimens softening and the beams yield in early stages. Furthermore, the vertical and the interface separation between the steel beam flange and the reinforced concrete slab are also noticed to increase and dominate significantly as a result of increasing beams span/radius ratio. Moreover, the failure of the beam changes from flexural to a combined effect of flexural and torsional, in which the beam twisting at mid-span become dominant and influential on the failure and beam behavior.

- The numerical models showed that when the stud number increased, there was a significant reduction in the interface separation between the steel flange and the reinforced concrete slab is obtained. Furthermore, the capacity of the specimens is observed with stud number increasing. About 30% in load is found for the beam with stud number 30, compared to the specimen with eight studs, due to the relative increase in the stiffness of the beams. Also, the flexural cracks in the concrete slab buttom surface gradually decrease to include the buttom middle area of the concrete slab under the loading surface and the stud area. Therefore, the strength and the stiffness of the stud shear connector must be considered in the inelastic analysis of curved steel-concrete composite beam.
- As the concrete compressive strength f_{cm} increased, the ductility of the section decreased, and the ultimate load capacity of the curved composite beam increased.
- The loading capacity and the curved composite beam yielding increased as the yield stress of the steel beam increased. For yield stress of 450 MPa, the load-carrying capacity was 143.78 kN; but for yield stress of 200 MPa, the load-carrying capacity was 90.82 kN (the load-carrying capacity is improved by 58.31%). The steel beam yield stress effect on the flexural cracks appears to be small and negligible on the bottom and top faces of the reinforced concrete slab, compared the other parameters.
- Based on the obtained results, the presence of web stiffeners with different locations in the curved composite beam affects the shear strength. It can be observed that the beam yielding began at an early stage when the stiffener number increase. The web twisting and vertical separation at the beam mid-span, are observed to decrease as the number of the stiffeners increases. Moreover, the existence of stiffeners with different locations has affected the crack progression in the slab and resulting in more crushing and flexural cracks at the span center.

Conflict of Interest

The authors confirm that there is no conflict of interest to declare for this publication.

Acknowledgements

The authors would like to express their sincere thanks to the editor and anonymous reviews for their time and valuable suggestions.

References

Abaqus, F.E.A. (2009). *ABAQUS analysis user's manual*. Dassault Systemes, Vélizy-Villacoublay, France.

AISC (2006). *A. 360-specification for structural steel buildings*. American Institute of Steel Construction. United States of America.

Byfield, M.P., Kemp, A.R., & Nethercot, D.A. (2002). Effect of strain hardening on flexural properties of steel beams. *The Structural Engineer*, *80*(8), 29-34.

Erkmen, R.E. & Bradford, M.A. (2009). Nonlinear elastic analysis of composite beams curved in-plan. *Engineering Structures*, *31*(7), 1613-1624.

Erkmen, R.E., & Bradford, M.A. (2011a). Nonlinear quasi-viscoelastic behavior of composite beams curved in-plan. *Journal of Engineering Mechanics*, *137*(4), 238-247.

Erkmen, R.E., & Bradford, M.A. (2011b). Time-dependent creep and shrinkage analysis of composite beams curved in-plan. *Computers & Structures*, *89*(1-2), 67-77.

Eurocode 2 (2004). *Design of concrete structures. part 1.1: general rules and rules for buildings*. British Standards Institution, London.

Eurocode 4 (2005). *Design of composite steel and concrete structures part 1.1: general rules and rules for buildings*. European Committee for Standardization, Brussels, Belgium.

Hibbit, H., Karlsson, B., & Sorensen, E.J.S. (2012a). *ABAQUS user manual version 6.12*. Simula, USA.

Hibbit, H., Karlsson, B., & Sorensen, E.J.S. (2012b). *Analysis user's manual volume IV*. Simula, USA.

Issa-El-Khoury, G., Linzell, D.G., & Geschwindner, L.F. (2014). Computational studies of horizontally curved, longitudinally stiffened, plate girder webs in flexure. *Journal of Constructional Steel Research*, *93*, 97-106.

Kim, W.S., Laman, J.A., & Linzell, D.G. (2007). Live load radial moment distribution for horizontally curved bridges. *Journal of Bridge Engineering*, *12*(6), 727-736.

Liang, Q.Q., & Uy, B. (2000). Theoretical study on the post-local buckling of steel plates in concrete-filled box columns. *Computers & Structures*, *75*(5), 479-490.

Liang, Q.Q., Uy, B., Wright, H.D., & Bradford, M.A. (2004). Local buckling of steel plates in double skin composite panels under biaxial compression and shear. *Journal of Structural Engineering*, *130*(3), 443-451.

Liew, J.Y.R., Thevendran, V., Shanmugam, N.E., & Tan, L.O. (1995). Behaviour and design of horizontally curved steel beams. *Journal of Constructional Steel Research*, *32*(1), 37-67.

Lin, W., & Yoda, T. (2014). Numerical study on horizontally curved steel-concrete composite beams subjected to hogging moment. *International Journal of Steel Structures*, *14*(3), 557-569.

Liu, X., Bradford, M.A., & Erkmen, R.E. (2013a). Time-dependent response of spatially curved steel-concrete composite members. I: computational modeling. *Journal of Structural Engineering*, *139*(12), 04013004.

Liu, X., Bradford, M.A., & Erkmen, R.E. (2013b). Time-dependent response of spatially curved steel-concrete composite members. II: curved-beam experimental modeling. *Journal of Structural Engineering*, *139*(12), 04013003.

Liu, X., Bradford, M.A., & Erkmen, R.E. (2013c). Non-linear inelastic analysis of steel-concrete composite beams curved in-plan. *Engineering Structure*, *57*, 484-492.

Nguyen, H.T., & Kim, S.E. (2009). Finite element modeling of push-out tests for large stud shear connectors. *Journal of Constructional Steel Research*, *65*(10-11), 1909-1920.

Pi, Y.L., Bradford, M.A., & Trahair, N.S. (2000). Inelastic analysis and behavior of steel I-beams curved in plan. *Journal of Structural Engineering*, *126*(7), 772-779.

Tan, E.L., & Uy, B. (2009). Experimental study on curved composite beams subjected to combined flexure and torsion. *Journal of Constructional Steel Research*, *65*(8-9), 1855-1863.

Tan, E.L., & Uy, B. (2011). Nonlinear analysis of composite beams subjected to combined flexure and torsion. *Journal of Constructional Steel Research*, *67*(5), 790-799.

Thevendran, V., Chen, S., Shanmugam, N.E., & Liew, J.Y.R. (1999). Nonlinear analysis of steel-concrete composite beams curved in plan. *Finite Elements in Analysis and Design*, *32*(3), 125-139.

Thevendran, V., Shanmugam, N.E., Chen, S., & Liew, J.Y.R. (2000). Experimental study on steel-concrete composite beams curved in plan. *Engineering Structures*, *22*(8), 877-889.

Yang, Y.B., & Kuo, S.R. (1987). Effect of curvature on stability of curved beams. *Journal of Structural Engineering*, *113*(6), 1185-1202.

Zhang, Y., Hou, Z., Li, Y., & Wang, Y. (2015). Torsional behaviour of curved composite beams in construction stage and diaphragm effects. *Journal of Constructional Steel Research*, *108*, 1-10.

Original content of this work is copyright © International Journal of Mathematical, Engineering and Management Sciences. Uses under the Creative Commons Attribution 4.0 International (CC BY 4.0) license at https://creativecommons.org/licenses/by/4.0/